The Surprising Power of Fragmentation: How Fuel Discontinuity Limits Wildfire Spread

by

Quinn Bitz

A Thesis Submitted in Partial Fulfillment of the
Requirements of the

HONOURS PROGRAM

in the School of Earth and Ocean Sciences

Supervisors: Jed O. Kaplan and Colin Goldblatt

University of Victoria

We acknowledge and respect the Lək̓ʷəŋən (Songhees and Xʷsepsəm/Esquimalt) Peoples on whose territory the university stands, and the Lək̓ʷəŋən and W̱SÁNEĆ Peoples whose historical relationships with the land continue to this day.

Abstract

Wildfire growth depends not only on the quantity of fuel but also on its continuity across the landscape (Keane et al., 2001; Pfeiffer et al., 2013). Fine-scale discontinuities such as roads, rivers, or rocky outcrops can halt fire progression, yet these features are often overlooked in large-scale fire models that treat fuels as homogeneous (Archibald et al., 2009; Bowman et al., 2020). This project investigates how fuel fragmentation at 30 m resolution constrains burned area in realistic landscapes.

Using the ELMFIRE fire spread model (Lautenberger, 2013) with LANDFIRE LF 2023 inputs (LANDFIRE, n.d.), I simulated nearly 8,000 ignition scenarios across five 60 × 60 km domains in the western United States. Burned and burnable area fractions were calculated for each 5 × 5 km tile (sub-domain) to quantify how fuel discontinuities interact with wind and landscape structure.

Results show that burned area increased exponentially across the full range of fuel continuity, forming an upper-limit relationship between burnable and burned area fractions. Fragmented landscapes rarely supported large-scale spread, defined here as cases where more than half of the burnable area was consumed. Wind speed had little effect under low connectivity, but in continuous fuels, stronger winds substantially amplified fire size. Other potential controls, including slope and vegetation structure, were weakly related to burned area, reinforcing fragmentation as the dominant limiting factor.

These findings demonstrate that fuel continuity imposes natural limits on wildfire growth, even under favourable weather. Incorporating such constraints into continental- and global-scale fire models could improve their ability to capture realistic spread dynamics in heterogeneous landscapes.

1. Introduction

The “fire environment triangle” was first outlined by Countryman (1972) and Pyne et al. (1996), emphasizing fuel, weather, and topography as interacting controls on wildfire. Moritz et al. (2005) reinforced this framing by demonstrating that these factors strongly influence wildfire growth at the scale of individual events. More recently, wildfire behaviour has been described in terms of a triad of fuel, weather, and ignition (Bowman et al., 2020; Higuera & Abatzoglou, 2021). This shift reflects recognition that, while topography modulates fire behaviour, ignition is the indispensable trigger that determines whether a fire occurs. In this project, I adopt the latter framing, treating wildfire growth as dependent on fuel, weather, and ignition.

Climatic conditions and ignition sources have been widely studied (Balch et al., 2017; Abatzoglou et al., 2018), yet fire cannot propagate without a continuous supply of burnable material (Keane et al., 2001; Pfeiffer et al., 2013). Even under favourable weather, fires may stall when non-burnable features such as roads, rocky outcrops, or bodies of water interrupt their path (Archibald et al., 2009; Bowman et al., 2020). Thus, the spatial structure and continuity of fuels are as important as their overall abundance (Keane et al., 2001; Bowman et al., 2020). The recent escalation in destructive wildfires underscores this point: fuels must not only exist but also be arranged in continuous patterns that allow fires to propagate across landscapes (Higuera & Abatzoglou, 2021; Kolden et al., 2024).

At fine spatial resolutions (1–10 m), landscapes are rarely continuous. Small gaps such as roads, cliffs, or creeks can interrupt fuel continuity and constrain fire growth (Atchley et al., 2021; Ritter et al., 2023). Burnable patches are interspersed with non-burnable features, creating fragmented mosaics (Pfeiffer, et al. 2013). Burned fraction tends to increase with wind speed but often levels off under moderate winds, when even a 10 m fire break can halt spread. This highlights that connectivity, rather than total fuel amount, governs sustained fire growth (Keane et al., 2001; Bowman et al., 2020; Frangieh et al., 2021).

By contrast, large-scale fire models are typically designed for continental to global simulations and run at coarse resolutions, from 50–100 km in Earth system fire models (Rabin et al., 2017) to 9 km in recent global forecasts (Di Giuseppe et al., 2025). Even when emissions are downscaled to 500 m (van Wees et al., 2022), fuels are homogenized, and fine-scale features such as downed logs, past disturbances, or small gaps that limit spread are overlooked (Keane et al., 2001; Bowman et al., 2020). This inconsistency creates a key modelling challenge: representing fine-scale spatial discontinuities within frameworks that must remain computationally efficient at broad scales.

Attempts to bridge this gap have required compromises. Many large-scale models, particularly those embedded in dynamic global vegetation models (DGVMs), rely on coarse assumptions, treating fuel as uniformly distributed and simulating ignition and spread using empirical or stochastic means calibrated to observations (Keane et al., 2004; Hantson et al., 2016). This approach allows global coverage but sacrifices the capacity to resolve how fine-scale fragmentation shapes fire perimeters (Rabin et al., 2017) or to represent unprecedented conditions such as extreme drought and heat. Intercomparison studies like FireMIP have revealed that differences in fuel continuity representation alone can lead to substantial variation in projected fire activity, even under identical climate inputs (Rabin et al., 2017). Similarly, attempts to link wind speed directly to burned area falter when spatial barriers disrupt spread (Lasslop et al., 2015). In Southern Africa, fragmentation from cultivation, grazing, and roads has been shown to reduce fire size and suppress burned area by breaking continuity, even where ignitions are abundant (Archibald et al., 2009; Archibald et al., 2010). These findings underscore the need for process-based simulations that retain realistic spatial patterns.

At regional to continental scales, studies such as Abatzoglou et al. (2018) demonstrate how interannual fire dynamics are shaped by climate variability, fuel aridity, and vegetation productivity. Yet these relationships often break down in fragmented landscapes, where physical discontinuities weaken the climate–fire link. This disconnect highlights a key challenge: coarse-resolution frameworks may reproduce aggregate fire outcomes, but not the mechanisms that constrain spread.

To address this gap, I apply ELMFIRE, a landscape-scale wildfire model that explicitly simulates fire growth at 30 m resolution (Lautenberger, 2013). This makes it well-suited for testing how fragmentation imposes emergent limits on fire growth. Observed fire perimeters provide valuable records, but they are strongly confounded by weather, ignition variability, and suppression efforts. Satellite-derived burned area datasets are also short and emphasize only certain metrics, limiting their ability to capture underlying processes (Archibald et al., 2013). By contrast, process-based models enable controlled experiments across thousands of landscapes, allowing fragmentation effects to be isolated and tested consistently (Lautenberger, 2013; Hantson et al., 2016).

Previous simulation efforts have hinted at threshold behaviour: Loehman et al. (2020) found that spatial arrangements of fuel can suppress fire occurrence, while Pfeiffer et al. (2013) showed that randomly distributed non-burnable land reduces average patch size nonlinearly, with continuity breaking down below ~40% burnable area. Bowring et al. (2024) used road density as a proxy for continuity, but at coarse 50 km grid scales, too large to capture landscape features such as cliffs or streams. These synthetic approaches are useful but call for empirical testing in real terrain (Hantson et al., 2016; Rabin et al., 2017).

Here I test whether such limiting patterns emerge in realistic landscapes. Using 30 m-resolution inputs, I simulate wildfire spread across five diverse domains, testing multiple ignition points and wind conditions to determine whether an upper bound on burned area emerges. This builds on Haas et al. (2022), who showed that road density and terrain ruggedness strongly constrain fire size, and on Kolden et al. (2024), who found that Canada's 2023 fire season saw extreme fire growth despite fewer ignitions, indicating that continuity, not ignition frequency, increasingly governs modern fire regimes. By quantifying fragmentation as the ratio of burnable to non-burnable pixels and linking it to burned area, I aim to identify a generalizable constraint on fire size. This could provide new insight into how structural fuel patterns limit growth under controlled meteorological conditions, supporting integration of fine-scale landscape structure into more scalable fire modelling approaches.

2. Methods

2.1 Study Design and Simulation Domains

I investigated how landscape characteristics influence simulated wildfire outcomes using the ELMFIRE wildfire spread model (Lautenberger, 2013). Five geographically distinct 60 × 60 km domains were selected in the forested inland Pacific Northwest of the United States (Figure 2.1). These areas represent a range of forest ecosystems, terrain complexity, and bioclimatic conditions, and many are situated in ecotonal regions where large-scale fire models often perform poorly (Hantson et al., 2016; Rabin et al., 2017; J. Kaplan, personal communication, July 2025). Ecotones such as forest–savanna boundaries highlight the ecological role of fire, where frequent grass-fueled burning maintains open savannas, and infrequent fire allows forest expansion (Higgins & Scheiter, 2012).

The ELMFIRE model requires input in the form of gridded spatial layers (rasters), which I sourced from the LANDFIRE LF 2023 dataset at 30 m resolution, a product currently only available for the United States (LANDFIRE, n.d.). Topographic inputs included digital elevation model (DEM), slope (SLP), and aspect (ASP). Vegetation structure was represented by canopy height (CH), canopy cover (CC), canopy base height (CBH), and canopy bulk density (CBD). Surface fuel types were provided by the Fire Behaviour Fuel Model 40 (FBFM40) raster (Scott & Burgan, 2005).

All rasters were clipped and aligned to the 60 × 60 km extent of each study area. To minimize edge effects on simulated fire spread, a 5 km buffer was retained on all sides. The central 50 × 50 km core was used for both simulations and statistical analyses (Figure 2.2). The experimental design was intended to test for nonlinear shifts in burned area across gradients of fuel availability and fragmentation (Loehman et al., 2020).

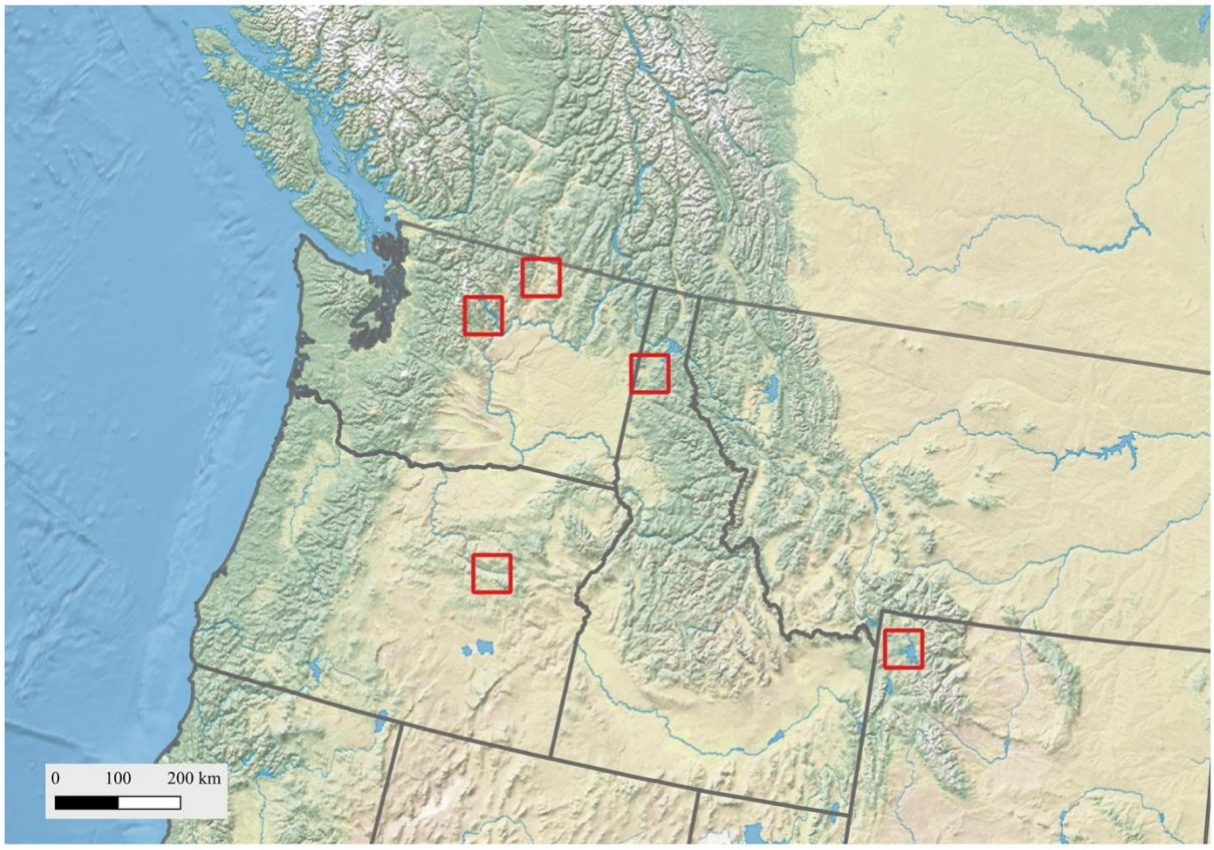

Figure 2.1. Five Study Area Locations Across the Northwestern United States.

Map showing the locations of the five 60 × 60 km study domains used in this analysis. Each red square represents a simulation region where wildfire spread was modelled using high-resolution terrain and vegetation inputs.

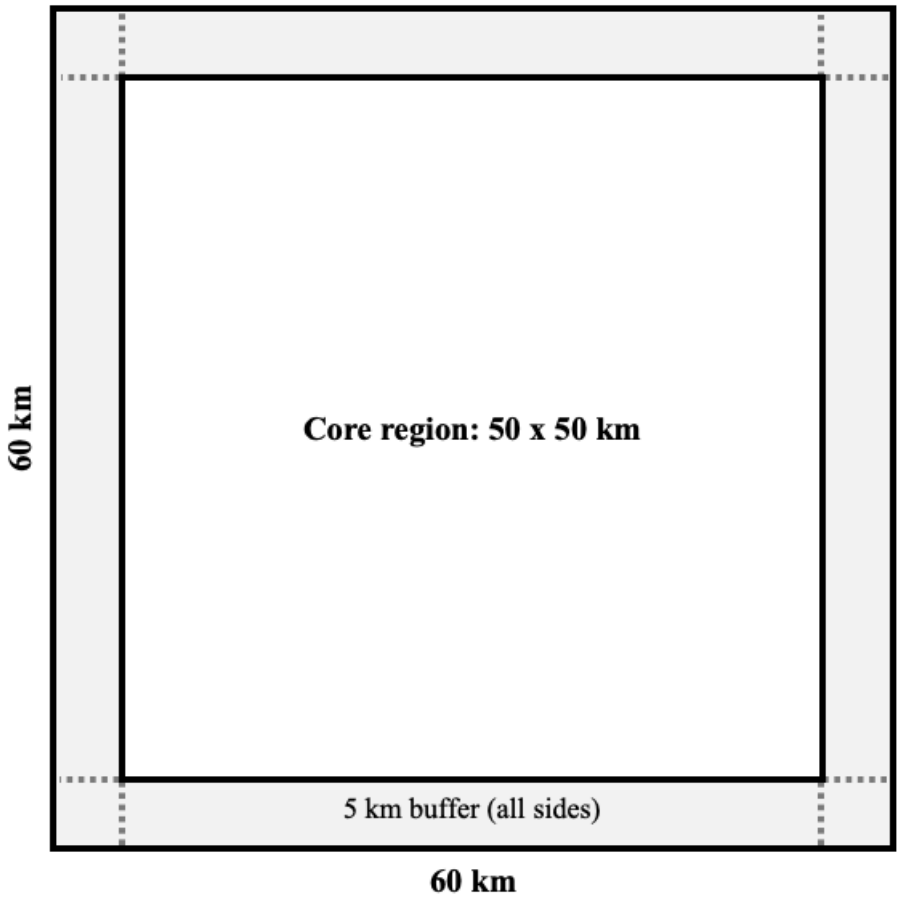

Figure 2.2. Schematic of study domain design.

Each study area measured 60 × 60 km in total, with a 5 km buffer around the edge and a 50 × 50 km core region used for simulations and statistical analyses.

2.2 Raster Classification and Burnable Area Identification

Burnable and non-burnable areas were classified using the Fire Behaviour Fuel Model 40 (FBFM40) raster, which encodes surface fuel types as integer values (Scott & Burgan, 2005). Burnable pixels were defined as those with FBFM40 codes ≥ 100, including grass (GR), grass–shrub (GS), shrub (SH), timber–understory (TU), and timber–litter (TL) fuel types. Non-burnable pixels included codes < 100, such as urban (91), agriculture (93), open water (98), and barren land (99), as well as pixels with the NoData value (32767).

Code Number in FBFM40 Raster	Abbreviation	Description
101–104	GR1–GR4	Grass types
121–123	GS1–GS3	Grass–shrub mixtures
141-148	SH1–SH7	Shrub types
161-165	TU1–TU5	Timber–understory combinations
181-189	TL1–TL9	Timber–litter types
<100	N/A	Non-burnable pixels

Table 1. Classification of burnable and non-burnable pixels based on FBFM40 raster codes (Scott & Burgan, 2005).

This classification approach is consistent with standard applications of fire behaviour fuel models in landscape-scale simulations, though it necessarily simplifies sub-pixel variability and within-class heterogeneity. Such generalizations reflect established trade-offs in fuel mapping between ecological realism and computational efficiency (Keane et al., 2001).

The burnable–non-burnable distinction was used to calculate burnable area fractions, restrict ignition point placement, and mask out non-burnable pixels during terrain and vegetation statistics calculations. Fragmentation was operationalized as the ratio of burnable to total pixels, reflecting growing recognition that spatial discontinuities in fuel constrain fire growth in ways often oversimplified in global fire models (Hantson et al., 2016).

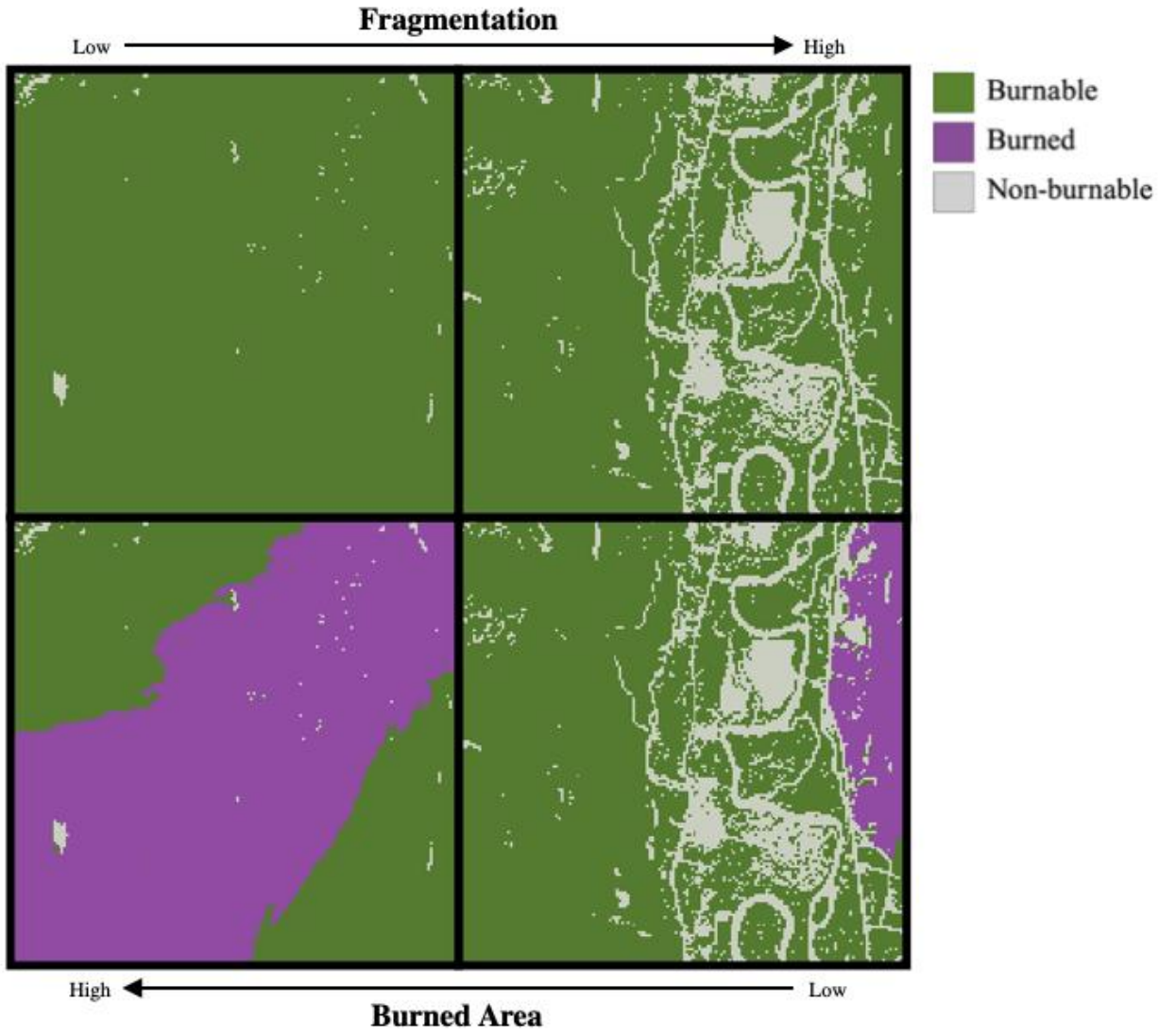

Figure 2.3. Schematic of Fragmentation and Fire Spread.

Conceptual schematic showing how burnable fuel continuity (fragmentation) and burned area interact in two example 5 × 5 km simulation tiles. Each column represents a distinct landscape tile with low (left) or high (right) non-burnable fragmentation. Each row shows the same tile before (top: fuel availability) and after (bottom: burned area) simulation. Green indicates burnable pixels, purple shows pixels that burned, and grey represents non-burnable areas. Burned area is highest in the lower-left panel and decreases toward the upper-right; fragmentation increases from left to right.

2.3 Ignition Protocol and Simulation Automation

Fires were ignited from the four corners of each 5 × 5 km tile: southwest (SW), southeast (SE), northeast (NE), and northwest (NW). Ignition points were placed 100 m inward from each corner to reduce edge effects (Figure 2.4). Ignitions were not pre-screened for burnability; if an ignition pixel fell within a non-burnable area, the simulation typically terminated without fire spread.

Simulations were automated using a master shell script (doall_areas_quads.sh), which called quadrant-specific scripts (e.g., doall5km_SWign.sh). ELMFIRE outputs included multiple raster layers, such as fireline intensity (FLIN). For this study, burned area was defined as any pixel with FLIN > 0. From this point forward, I refer simply to burned area in describing results.

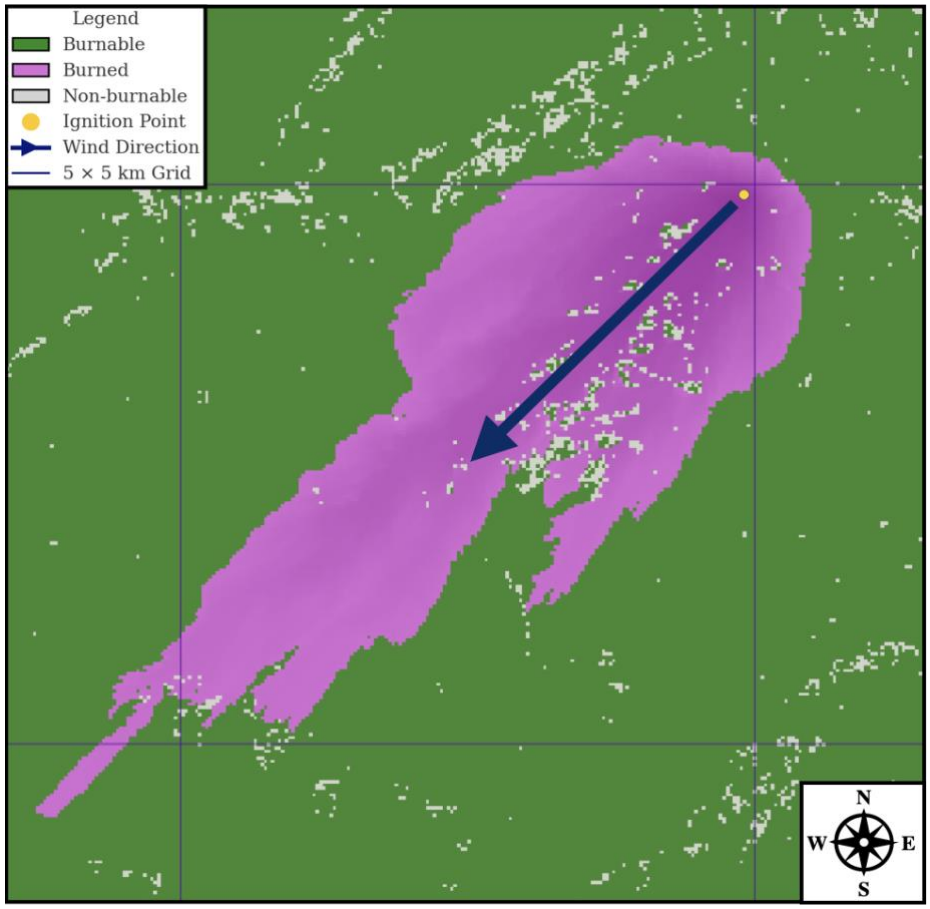

Figure 2.4. Example Fire Simulation – Northern Washington, 15 mph Northeasterly Wind. Simulated wildfire spread in a 60 × 60 km tile located in northern Washington. The ignition point is marked in yellow, and the blue arrow indicates a 15 mph (≈ 6.7 m s^{-1}) northeasterly wind. The resulting

burned area (magenta) spreads toward the southwest across a heterogeneous fuel landscape, with burnable areas shown in green and non-burnable areas in light grey. The domain is divided into 5 × 5 km analysis tiles, shown by the blue grid overlay.

2.4 ELMFIRE Model Setup

The ELMFIRE model is a physics-based wildfire spread simulator that predicts fire growth using gridded terrain, fuel, and weather inputs (Lautenberger, 2013). It employs a level set method, a numerical scheme for evolving moving boundaries (Osher & Sethian, 1988), to simulate fire perimeters. This approach has been widely applied to wildfire modelling (Fendell & Wolff, 2001; Rehm & Mell, 2009) and is implemented directly in ELMFIRE.

In this study, wind speed and fuel moisture were held constant to isolate fragmentation effects. While ELMFIRE can be driven with time-varying meteorological inputs, this represents a design choice rather than a model limitation (Lautenberger, 2013).. The model does not simulate fire–atmosphere feedbacks, such as fire-generated winds or plume dynamics. This simplification makes ELMFIRE well suited for testing how fixed landscape structure constrains surface fire spread under controlled conditions.

Simulations used a fixed 24-hour burn period and constant input conditions. Wind speeds of 15, 30, 45, and 60 mph (6.7, 13.4, 20.1, and 26.8 m s^{-1}) were applied from fixed cardinal directions. These values span moderate to extreme fire weather scenarios, with the upper end representing rare but plausible events. ELMFIRE requires wind speed inputs in miles per hour (Lautenberger, 2013), results are reported here in SI units. Fixing wind speed and ignition direction across all runs enabled clearer isolation of landscape effects, addressing a common limitation in coarser-scale models where wind–fire relationships saturate or reverse due to unresolved sub-grid processes (Lasslop et al., 2015).

Terrain and fuel inputs were drawn from the LANDFIRE LF 2023 dataset (LANDFIRE, n.d.). A consistent ELMFIRE namelist template was used for each run to specify input file paths and domain

properties. No stochastic elements were introduced in ignition placement or simulation setup, and all runs are fully reproducible. Simulations terminated automatically when flame front intensity could not be sustained, a mechanism conceptually similar to other spatial fire models, such as FireBGCv2, which halts spread at fuel discontinuities or landscape boundaries (Loehman et al., 2020).

2.5 Burned Area and Terrain Variable Analysis

Each 60 × 60 km domain was divided into 100 non-overlapping 5 × 5 km tiles (167 × 167 pixels). For each tile, I calculated three metrics:

(i) Burnable Area Fraction: burnable pixels ÷ total pixels

(ii) Burned Area Fraction: burned pixels ÷ total pixels

(iii) Adjusted Burned Area Fraction: burned pixels ÷ burnable pixels (capped at 1.0).

Tiles with no burnable pixels (e.g., in Yellowstone Lake) were excluded from analysis. The FBFM40 fuel type raster was masked using the burnable pixel filter, while the other seven landscape variables (ASP, SLP, DEM, CBD, CBH, CC, and CH) were summarized directly. All variables, previously defined, are listed in Table 2 for reference.

Variable	Description
ASP	Aspect (degrees)
SLP	Slope (degrees)
DEM	Digital Elevation Model (m)
CBD	Canopy Bulk Density (kg m^{-3})
CBH	Canopy Base Height (m)
CC	Canopy Cover (%)
CH	Canopy Height (m)
FBFM40	Fire Behavior Fuel Model 40 code classification

Table 2. Landscape variables used in the analysis and their descriptions. All variables were derived from the LANDFIRE LF 2023 dataset.

Within each tile, five descriptive statistics were calculated for every landscape variable: mean, median, standard deviation, and skewness. These metrics were compiled into a single dataset that linked tile-level variables with simulation metadata, including wind speed, ignition direction, and study area.

In total, 8,000 simulations were conducted, spanning all combinations of five regions × 100 tiles × four ignition points × four wind speeds. Sixteen runs were excluded due to invalid ignition points or tiles with no burnable pixels (e.g., Yellowstone Lake), resulting in 7,984 valid simulations for analysis (Table 3).

Parameter	**Values**
Study areas	5
Tiles per area	100
Ignition directions (SW, SE, NE, NW)	4
Wind speeds (15, 30, 45, 60 mph)	4
Total simulations	5 × 100 × 4 × 4 = 8000
Valid entries	7984

Table 3. Simulation design overview. A total of 8,000 simulations were generated; 7,984 valid entries were retained after excluding 16 runs with invalid ignition points or tiles lacking burnable pixels.

2.6 Statistical Analyses

All statistical analyses and visualizations were conducted in Python 3.12.3 using core scientific libraries: NumPy, Pandas, SciPy, Scikit-learn, Rasterio, Matplotlib, Seaborn, and itertools. The primary objective was to assess how fuel continuity, terrain characteristics, and wind speed interact to shape fire spread potential, with the main outcome variable being the Adjusted Burned Area Fraction.

Three analytical approaches were applied. First, exploratory visualizations and descriptive statistics were used to characterize relationships between burnable area fraction and fire outcomes. Scatterplots and summary metrics (mean, median, variance, skewness) provided an initial assessment of overall patterns.

Second, an exponential curve was fitted to the 95th percentile upper envelope of Adjusted Burned Area Fraction values, calculated across 1% bins of burnable fraction. This analysis quantified maximum spread potential at different levels of fuel continuity and revealed an emergent exponential upper bound. For descriptive purposes, "large-scale spread" was defined as cases where ≥ 50% of the tile area burned, which generally corresponded to burnable fractions of ~0.8 or higher. This threshold was used only to structure results.

Third, tiles were grouped into Low Fragmentation (burnable fraction ≥ 0.8) and High Fragmentation (< 0.8) categories. Boxplots were then used to compare fire outcomes across wind speeds of 15, 30, 45, and 60 mph (6.7, 13.4, 20.1, and 26.8 m s^{-1}) within each fragmentation group. Mann–Whitney U-tests (both one-sided and two-sided) were applied to assess statistical significance between wind speed categories.

Finally, relationships between terrain and vegetation structure and fire outcomes were explored using scatterplots and two-dimensional kernel density estimation (KDE) contour plots, which highlight regions of higher point density (Appendix A). Summary statistics (mean, median, standard deviation, skewness) of key variables, including canopy height, canopy cover, canopy base height, canopy bulk density, slope, and elevation, were compared against Adjusted Burned Area Fraction.

All analyses were performed tile-wise on the cleaned dataset of 7,984 valid simulations, with figures presented in the Results section and Appendix A.

3. Results

3.1 Burnable Area and Fire Spread: Evidence of a Nonlinear Relationship

Across all 7,984 valid 5 × 5 km simulation tiles, the relationship between burnable area fraction and burned area fraction was strongly nonlinear. Most tiles exhibited substantially less burning than their total fuel availability would suggest. A two-dimensional kernel density estimate (KDE) showed that the majority of simulations clustered well below the 1:1 line, indicating that even in landscapes with near-continuous fuel, realized burned area was often constrained (Figure 3.1).

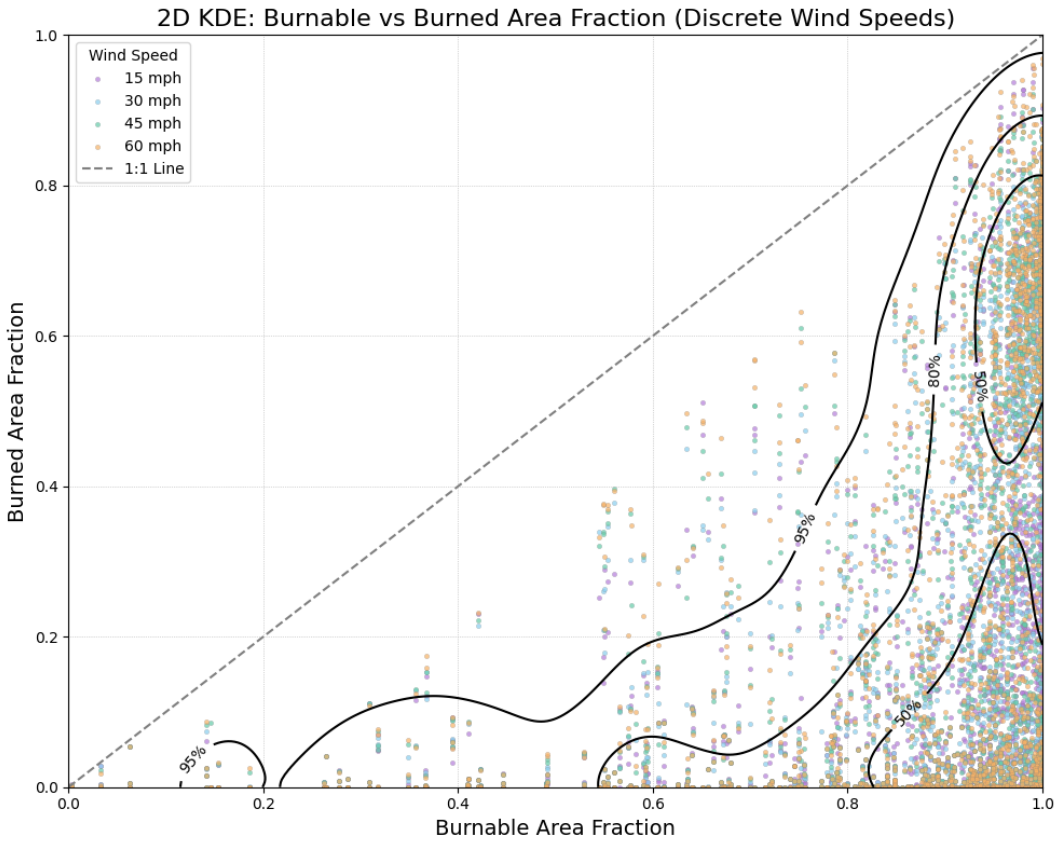

Figure 3.1. Joint distribution of burnable and burned area fractions across all 5×5 km simulation tiles (n = 7,984).

Coloured points show individual simulations, and black contour lines indicate a two-dimensional kernel density estimate (KDE), with contours representing the 50%, 80%, and 95% highest-density regions. The dashed line marks the 1:1 relationship. Most tiles fall well below this line, indicating that even in areas with high burnable fuel availability, actual burned area is often lower due to constraints.

To quantify the relationship between burnable and burned area fractions, I calculated median burned area fractions within 5% bins of burnable area. Median values increased with higher burnable fractions and were best captured by an exponential model, which substantially outperformed a linear alternative (Figure 3.2). This analysis demonstrates that central tendencies in the data are nonlinear, reinforcing the need for nonlinear approaches to evaluate fuel continuity effects and providing the basis for shifting to adjusted metrics and upper-bound analyses in subsequent sections.

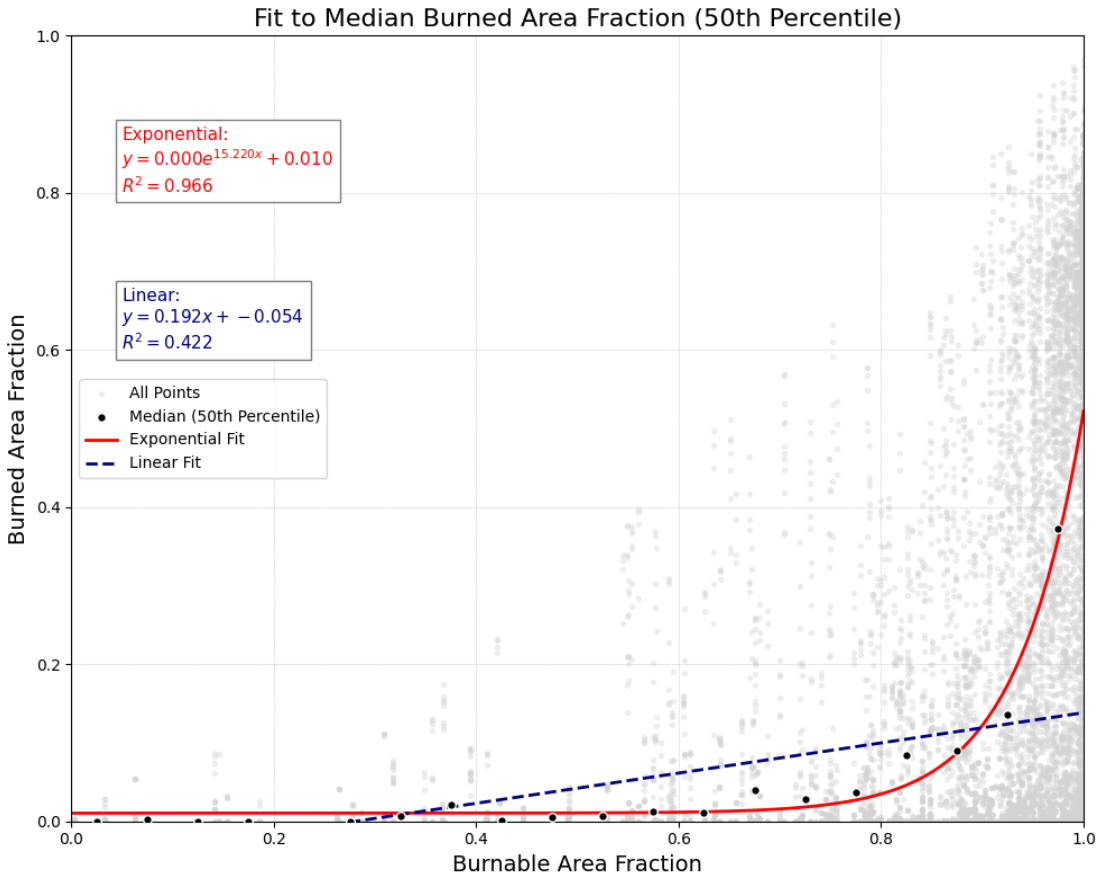

Figure 3.2. Relationship between burnable and burned area fractions across simulation tiles, summarized using binned medians.

Black points show the 50th percentile of burned area in 5% burnable fraction bins. The exponential model (red) provides a strong fit ($R^2 = 0.966$), outperforming the linear alternative (blue dashed, $R^2 = 0.422$). This non-linear relationship supports the use of adjusted burned area metrics and envelope-based analyses in later sections.

To estimate a theoretical maximum for fire spread under optimal conditions, I applied a quantile regression approach following Archibald et al. (2009). The resulting exponential fit ($R^2 = 0.889$) revealed a clear upper limit, with spread potential increasing exponentially across the full range of burnable fractions (Figure 3.3). For comparison, a linear fit to the same 95th percentile envelope (Figure A.1) produced a reasonably strong correlation ($R^2 = 0.826$) but failed to capture the curvature of the upper-limit relationship, reinforcing the suitability of the exponential form.

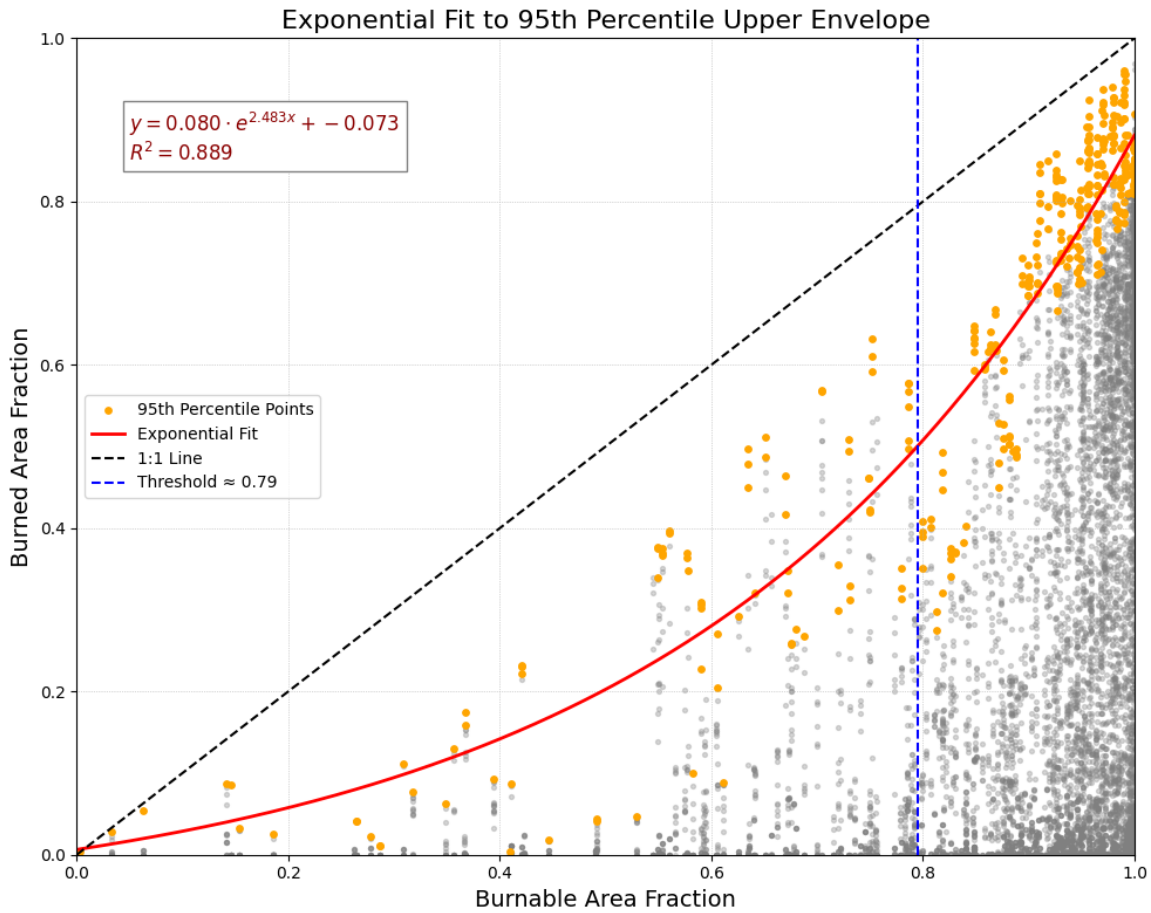

Figure 3.3. Exponential model fitted to the 95th percentile upper envelope of burned area fraction. Orange points represent the top 5% of fire spread within each 1% bin of burnable area fraction. The exponential fit ($R^2 = 0.889$) captures the nonlinear increase in spread potential with increasing fuel continuity. A vertical dashed line marks the continuity level (burnable fraction ≈ 0.79) at which the modeled upper-envelope crosses 50% burned area.

In this study, large-scale spread is defined as cases where more than 50% of the tile area burned. This descriptive cutoff, indicated by the vertical dashed line in Figure 3.3, corresponds to burnable fractions of roughly 0.8 in the most permissive simulations and is used only to guide interpretation. Below ~0.8 burnable fraction, the modeled 95th-percentile upper envelope remains under 50% burned area; above ~0.8, it exceeds 50%, marking where large-scale spread becomes feasible in this setup.

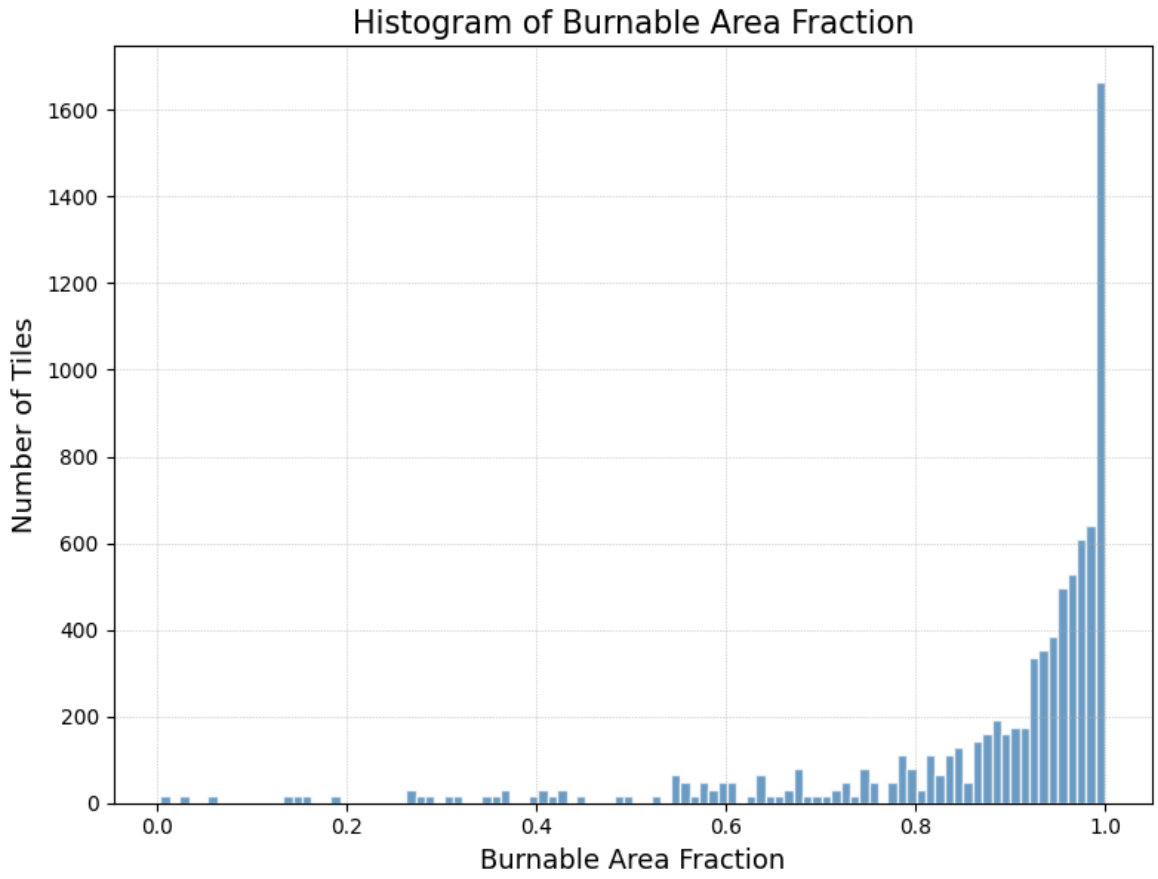

Figure 3.4. Histogram of burnable area fractions across all simulated 5 × 5 km tiles (n = 7,984). The distribution is strongly skewed toward values near 1.0, reflecting the generally forested nature of the study regions and indicating low fragmentation and high fuel availability.

The distribution of burnable area fractions across all tiles was strongly right-skewed toward values near 1.0, reflecting the generally forested nature of the study regions (Figure 3.4). Although many tiles had

high fuel availability, relatively few achieved burned areas close to the theoretical 1:1 maximum (Figure 3.3). This indicates that most fires consumed less area than fuel continuity alone would permit.

3.2 Wind Speed Effects Vary by Fragmentation Level

To assess whether wind influenced fire outcomes differently in fragmented versus continuous landscapes, simulation tiles were grouped into two categories: low fragmentation (burnable fraction ≥ 0.8) and high fragmentation (< 0.8). In high-fragmentation landscapes, adjusted burned area fractions remained consistently low across all wind speeds, showing that disconnected fuels constrained spread regardless of atmospheric conditions. In contrast, low-fragmentation landscapes exhibited a clear increase in burned area with rising wind speed, demonstrating that continuous fuels enabled stronger wind-driven propagation (Figure 3.5)

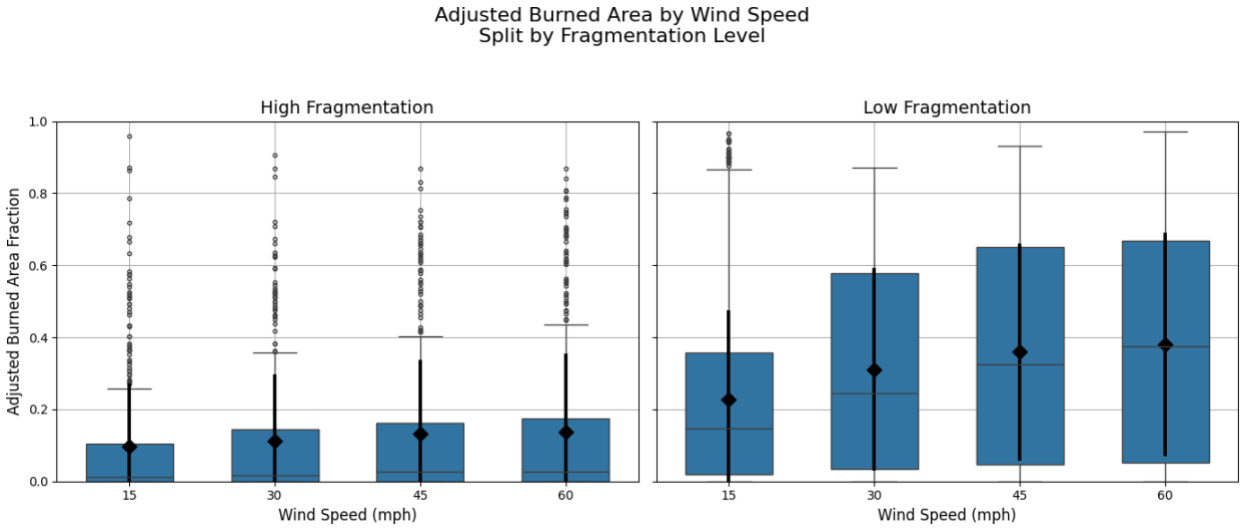

Figure 3.5. Boxplots of adjusted burned area fraction by wind speed, stratified by fuel fragmentation level.

Tiles with burnable area fraction > 0.8 are categorized as low fragmentation (high fuel continuity). In high-fragmentation landscapes, wind speed has minimal effect on fire spread. In contrast, low-fragmentation regions show marked increases in burned area with higher wind speeds, highlighting the role of fuel continuity in enabling wind-driven fire propagation.

To test the statistical significance of these trends, I performed a series of one-sided Mann–Whitney U-tests, evaluating the directional hypothesis that burned area fraction increases with wind speed within each fragmentation group. In low-fragmentation tiles, nearly all pairwise wind speed comparisons were significant ($p < 0.05$), confirming a strong positive relationship between wind and fire spread (Figure 3.6). In contrast, high-fragmentation landscapes showed only a few significant comparisons, and the pattern was inconsistent, indicating that discontinuous fuels dampened the effect of wind.

Directional Hypothesis: Fire Spread Increases with Wind Speed
Mann–Whitney U-Test (One-Sided)

Low Fragmentation

	15	30	45	60
15				
30	0.000*			
45	0.000*	0.000*		
60	0.000*	0.000*	0.037*	

High Fragmentation

	15	30	45	60
15				
30	0.168			
45	0.042*	0.215		
60	0.036*	0.195	0.461	

Figure 3.6. One-sided Mann–Whitney U-test comparing adjusted burned area fractions across increasing wind speeds, separately for low and high fragmentation levels.

P-values test the directional hypothesis that fire spread increases with wind speed. In low-fragmentation landscapes, nearly all comparisons are statistically significant ($p < 0.05$), supporting a strong positive effect of wind. In contrast, high-fragmentation areas show limited and inconsistent significance, indicating that fragmented fuels may constrain spread even under higher wind conditions.

These findings were consistent with more conservative two-sided Mann–Whitney U-tests, which also showed widespread significance in low-fragmentation areas but minimal effects in fragmented terrain (Figure A.2). Taken together, the results highlight that while wind speed is a dominant control in landscapes with continuous fuels, its influence is limited when connectivity thresholds are not met.

3.3 Terrain and Vegetation Metrics Show No Simple Predictors

To test whether landscape structure beyond fuel continuity influenced fire outcomes, I compared results from the least fragmented landscapes (burnable fraction ≥ 0.8) with those from the full dataset. Restricting to high-continuity tiles allowed terrain and vegetation effects to be examined without the overriding influence of fragmentation. In both cases, kernel density estimates were used to assess relationships between adjusted burned area fraction and tile-level summary statistics (mean, median, standard deviation, and skewness) for canopy height, canopy cover, canopy base height, canopy bulk density, slope, elevation, and aspect.

Across all variable–statistic combinations, no strong trends were apparent. Higher burned areas occasionally coincided with moderate canopy heights or slope values, but such density hotspots were rare. Overall, the distributions were diffuse and lacked consistent structure (Figure A.3). This suggests that these variables, when considered independently, are not reliable predictors of burned area at the 5 × 5 km scale under constant wind and ignition conditions.

Instead, terrain and vegetation metrics appear to shape fire behaviour through more complex, multivariate interactions or threshold effects not captured by pairwise density plots. Even so, they provided important context for describing study area heterogeneity and guided data filtering and tile characterization throughout the analysis.

4. Discussion

4.1 Fragmentation as a Limiting Control on Fire Spread

This study confirms that landscape fragmentation strongly constrains burned area, even when fuel abundance and meteorological conditions are favourable. Fires rarely propagated broadly in highly fragmented tiles, and even in more continuous landscapes, maximum spread was seldom achieved. These findings demonstrate that the spatial continuity of wildfire fuels, not simply their overall quantity, plays a primary role in limiting fire size.

This conclusion aligns with global findings by Bowman et al. (2020), Haas et al. (2022), and Higuera & Abatzoglou (2021), who show that fragmentation caused by terrain, land use, or vegetation type can suppress fire activity even in highly flammable settings. Similarly, Pfeiffer et al. (2013) demonstrated that fire spread in synthetic landscapes collapses once connectivity declines beyond a critical point. My results exhibit the same general pattern, but the key outcome here is not the identification of a fixed threshold. Rather, it is the consistent demonstration that fragmentation reduces fire growth across a wide range of conditions.

4.2 Interpretation of the Exponential Quantile Regression

The exponential quantile regression fitted to the 95th percentile upper envelope provided a strong approximation of maximum spread potential under idealized conditions. Importantly, this emergent exponential relationship is more than descriptive: it offers a tractable way to represent fragmentation effects in larger-scale models. By quantifying how burned area scales with fuel continuity, these results provide a pathway to parameterize fragmentation in coarse-resolution fire modules, which currently lack mechanisms to capture fine-scale structural limits on spread.

For interpretation, I defined large-scale spread as cases where ≥ 50% of the tile area burned, which typically occurred only in landscapes with high fuel continuity. This operational cutoff was used solely

for communication, not as a universal ecological limit. The dataset was also skewed toward fuel-rich environments: only 18.4% of simulation tiles (1,472 of 7,984) fell into the high-fragmentation category. This imbalance reduces the robustness of the fit in fragmented landscapes and highlights the need for future studies to sample more evenly across the full spectrum of fuel continuity.

Upper-limit relationships between environmental constraints and burned area have been observed in both empirical and simulation studies. Archibald et al. (2009) used quantile methods to detect spread-limiting thresholds under varying climate and fuel conditions, while Pfeiffer et al. (2013) showed that randomly distributed non-burnable land reduces patch size nonlinearly, with continuity breaking down below ~40%. Duane et al. (2021) likewise identified percolation-based thresholds in the 0.4–0.8 range of connectivity, above which structural barriers ceased to constrain growth. My exponential envelope is consistent with these patterns, reinforcing fragmentation as a fundamental limit on spread, though I emphasize that no single cutoff should be treated as universal.

Loehman et al. (2020) also observed nonlinear shifts in fire outcomes once connectivity falls below critical levels. My results align with this broader insight but avoid assigning significance to a single threshold value. Previous studies such as Hantson et al. (2016) and Lasslop et al. (2015) incorporated fixed spread thresholds into large-scale models, but these were often imposed empirically rather than derived from landscape structure. The current findings suggest that such limits may instead emerge naturally from high-resolution simulations of realistic terrain, providing a stronger foundation for parameterizing fire spread constraints in coarse-scale models using empirically grounded relationships rather than static assumptions.

4.3 Wind Effects and Meteorological Assumptions

In this study, fire spread was simulated under constant meteorological forcing: each ignition was exposed to a fixed wind speed and direction for a continuous 24-hour period. While such conditions are plausible during extreme fire events, they are not typical of most wildfires, where wind fluctuates with diurnal and

synoptic cycles and interacts strongly with terrain (Lasslop et al., 2015; Bowman et al., 2020; Higuera & Abatzoglou, 2021). The use of static boundary conditions likely amplified the role of wind in my simulations, particularly in low-fragmentation landscapes. However, this was an intentional design choice to isolate fragmentation effects rather than a limitation of the model. ELMFIRE is capable of incorporating dynamic meteorological inputs (Lautenberger, 2013).

The interaction between wind and fragmentation observed here is consistent with both simulation and observational research. Haas et al. (2022), Bowring et al. (2024), and Kolden et al. (2024) emphasize that wind-driven spread depends critically on fuel continuity. In fragmented landscapes, high winds fail to amplify growth because there are no continuous fuels to propagate the flame front. This mirrors recent extreme fire events, such as those in Chile and Hawai‘i, where high winds produced rapid spread only in areas with connected vegetation (Kolden et al., 2024). Similarly, Lasslop et al. (2015) found that burned area plateaus or even declines at high wind speeds, which they attributed to fragmentation or suppression mechanisms not captured in coarse-resolution models.

These interaction effects were further confirmed by statistical testing. One-sided Mann–Whitney U-tests showed significant differences in adjusted burned area fraction across wind speeds within low-fragmentation tiles, indicating that wind enhanced fire spread when fuels were continuous. In contrast, high-fragmentation landscapes showed few significant differences, reinforcing the interpretation that fragmentation disrupts the capacity of wind to drive fire growth. This conclusion aligns with prior modelling work suggesting that fuel connectivity is a stronger constraint on spread than meteorological drivers (Bowring et al., 2024; Haas et al., 2022).

4.4 Fuel Moisture and Static Inputs

A second major simplification in this study is the treatment of fuel moisture. All simulations assumed spatially uniform, constant fuel moisture across the landscape. This ignores important variability driven by slope, aspect, and microclimate, as in the Northern Hemisphere, north-facing slopes are typically

cooler and moister than south-facing slopes. By omitting this heterogeneity, the analysis may have overestimated fire spread in some settings while underestimating it in others.

Future studies should incorporate spatially heterogeneous or time-varying fuel moisture inputs to better reflect real-world conditions. As Keane et al. (2004) note, many landscape fire succession models (LFSMs) also simplify fuel moisture, limiting their realism in simulating spatial fire behaviour. Integrating more dynamic moisture representations would strengthen the ecological realism of simulations and improve the applicability of fragmentation constraints under diverse burning conditions.

4.5 Model and Domain Limitations

ELMFIRE was adopted in this study without direct validation or calibration. Although it has been applied in peer-reviewed literature (Lautenberger, 2013), I did not evaluate its performance against empirical fire perimeters or observational benchmarks. This leaves open the possibility that the model may systematically over- or underestimate spread under certain conditions. Lautenberger (2013) demonstrated how spatial discontinuities captured by LANDFIRE can limit fire spread; the current study extends this principle into a broader statistical relationship.

The five simulation domains were selected to represent a range of mostly forested landscapes in the inland Pacific Northwest. While consistent patterns emerged across these regions, the exponential fragmentation–spread relationship identified here cannot be assumed to be universal. As Keane et al. (2001, 2004) note, many fire models struggle to generalize across landscapes due to heterogeneity in fuel structure, climate, and topography. Further testing in different ecoregions is needed to determine whether the ~0.8 threshold observed here also applies in more fragmented, wetter, grassier, or more urbanized environments.

Finally, while LANDFIRE provides one of the most detailed and consistent fine-scale fuel datasets currently available, comparable products are rare outside the United States. This limits the ability to test

fragmentation effects globally and underscores the need for more spatially explicit fuel mapping in other regions (Hantson et al., 2016; Rabin et al., 2017).

4.6 Treatment of Non-Burnable Areas

Built-up areas such as cities, roads, and agricultural zones were classified as non-burnable in this study, following standard FBFM40 code groupings (Scott & Burgan, 2005). However, recent wildfires in California, Fort McMurray (Alberta), and Lahaina (Hawai‘i) have shown that fire can spread through suburban and urban areas, particularly when embers ignite structures or dry vegetation within the wildland–urban interface (WUI) (Keeley & Syphard, 2019; Higuera & Abatzoglou, 2020). Bowman et al. (2020) note that fragmentation from roads and land-use change can reduce fire spread, but only up to a point. Under extreme conditions, areas classified as “non-burnable” may themselves become pathways for propagation. Future work should explore more flexible classification schemes or conditionally flammable categories to better capture WUI dynamics.

Overall, the Discussion underscores a central point: fragmentation consistently limits fire growth, but its expression depends on modelling choices and landscape context. The following Conclusion brings together these findings and their broader implications.

5. Conclusion

My research demonstrates that landscape fragmentation imposes a strong limiting control on wildfire spread, even under favourable weather conditions. Using nearly 8,000 high-resolution simulations with the ELMFIRE model, I showed that burned area scales nonlinearly with fuel continuity, following an exponential upper bound. Fires rarely achieved maximum spread, and fragmentation consistently muted the influence of wind, confirming that weather alone is not sufficient to drive large-scale fire growth when structural fuel barriers are present.

By resolving fuel continuity at 30 m resolution, this study extends threshold-based theoretical insights into realistic terrain and vegetation settings. The emergent exponential relationship provides an empirically grounded way to parameterize fragmentation effects in continental- and global-scale fire models, which currently homogenize fuels and often overestimate spread in heterogeneous landscapes. Other landscape metrics, such as slope and canopy structure, showed only weak individual correlations with fire outcomes, underscoring burnable fraction as the dominant predictor of spread potential.

These findings highlight a critical opportunity for model development. Incorporating fragmentation constraints into coarse-scale frameworks could improve the realism of global fire forecasting while maintaining computational efficiency. Future research should test whether the exponential scaling relationship holds across different ecosystems and fuel types and evaluate its performance against observed fire perimeters. Taken together, this work provides a foundation for bridging high-resolution fire dynamics with global fire modelling, ensuring that fragmentation, fuel continuity, and spatial structure are no longer overlooked in a rapidly changing fire regime.

References

Abatzoglou, J. T., Williams, A. P., Boschetti, L., Zubkova, M., & Kolden, C. A. (2018). Global patterns of interannual climate–fire relationships. *Global Change Biology*, *24*(11), 5164–5175. doi: 10.1111/gcb.14405

Archibald, S., Roy, D. P., Van Wilgen, B. W., & Scholes, R. J. (2009). What limits fire? an examination of drivers of burnt area in Southern Africa. *Global Change Biology*, *15*(3), 613–630. doi: 10.1111/j.1365-2486.2008.01754.x

Archibald, S., Scholes, R. J., Roy, D. P., Roberts, G., & Boschetti, L. (2010). Southern African fire regimes as revealed by Remote Sensing. *International Journal of Wildland Fire*, *19*(7), 861. doi: 10.1071/wf10008

Archibald, Sally, Lehmann, C. E., Gómez-Dans, J. L., & Bradstock, R. A. (2013). Defining pyromes and global syndromes of fire regimes. *Proceedings of the National Academy of Sciences*, *110*(16), 6442–6447. doi: 10.1073/pnas.1211466110

Atchley, A. L., Linn, R., Jonko, A., Hoffman, C., Hyman, J. D., Pimont, F., Sieg, C., & Middleton, R. S. (2021). Effects of fuel spatial distribution on wildland fire behaviour. *International Journal of Wildland Fire*, *30*(3), 179. doi: 10.1071/wf20096

Balch, J. K., Bradley, B. A., Abatzoglou, J. T., Nagy, R. C., Fusco, E. J., & Mahood, A. L. (2017). Human-started wildfires expand the fire niche across the United States. *Proceedings of the National Academy of Sciences*, *114*(11), 2946–2951. doi: 10.1073/pnas.1617394114

Bowman, D. M., Kolden, C. A., Abatzoglou, J. T., Johnston, F. H., van der Werf, G. R., & Flannigan, M. (2020). Vegetation fires in the anthropocene. *Nature Reviews Earth & Environment*, *1*(10), 500–515. doi: 10.1038/s43017-020-0085-3

Bowring, S. P., Li, W., Mouillot, F., Rosan, T. M., & Ciais, P. (2024). Road fragment edges enhance wildfire incidence and intensity, while suppressing global burned area. *Nature Communications*, *15*(1). doi: 10.1038/s41467-024-53460-6

Countryman, C. M. (1972). The Fire Environment Concept (U.S. Department of Agriculture Forest Service Pacific Southwest Forest and Range Experiment Station, Berkeley, CA).

Di Giuseppe, F., McNorton, J., Lombardi, A., & Wetterhall, F. (2025). Global data-driven prediction of fire activity. *Nature Communications*, *16*(1). doi: 10.1038/s41467-025-58097-7

Duane, A., Miranda, M. D., & Brotons, L. (2021). Forest connectivity percolation thresholds for fire spread under different weather conditions. *Forest Ecology and Management*, *498*, 119558. doi: 10.1016/j.foreco.2021.119558

Fendell, F. E., & Wolff, M. F. (2001). Wind-aided fire spread. In E. A. Johnson & K. Miyanishi (Eds.), Forest fires: Behavior and ecological effects (pp. 171–223). Academic Press.

Frangieh, N., Accary, G., Rossi, J.-L., Morvan, D., Meradji, S., Marcelli, T., & Chatelon, F.-J. (2021). Fuelbreak effectiveness against wind-driven and plume-dominated fires: A 3D numerical study. *Fire Safety Journal*, *124*, 103383. doi: 10.1016/j.firesaf.2021.103383

Full extent downloads. LandFire. (n.d.). https://landfire.gov/data/FullExtentDownloads?field_version_target_id=All&field_theme_target_id=All&field_region_id_target_id=4

Haas, O., Prentice, I. C., & Harrison, S. P. (2022). Global Environmental Controls on wildfire burnt area, size, and intensity. *Environmental Research Letters*, *17*(6), 065004. doi: 10.1088/1748-9326/ac6a69

Hantson, S., Arneth, A., Harrison, S. P., Kelley, D. I., Prentice, I. C., Rabin, S. S., Archibald, S., Mouillot, F., Arnold, S. R., Artaxo, P., Bachelet, D., Ciais, P., Forrest, M., Friedlingstein, P., Hickler, T., Kaplan, J. O., Kloster, S., Knorr, W., Lasslop, G., … Yue, C. (2016). The status and challenge of global fire modelling. *Biogeosciences*, *13*(11), 3359–3375. doi: 10.5194/bg-13-3359-2016

Higgins, S. I., & Scheiter, S. (2012). Atmospheric CO2 forces abrupt vegetation shifts locally, but not globally. *Nature*, *488*(7410), 209–212. doi: 10.1038/nature11238

Higuera, P. E., & Abatzoglou, J. T. (2020). Record-setting climate enabled the extraordinary 2020 fire season in the Western United States. *Global Change Biology*, *27*(1), 1–2. doi: 10.1111/gcb.15388

Keane, R. E., Burgan, R., & van Wagtendonk, J. (2001). Mapping wildland fuels for fire management across multiple scales: Integrating Remote Sensing, GIS, and Biophysical Modeling. *International Journal of Wildland Fire*, *10*(4), 301–319. doi: 10.1071/wf01028

Keane, R. E., Cary, G. J., Davies, I. D., Flannigan, M. D., Gardner, R. H., Lavorel, S., Lenihan, J. M., Li, C., & Rupp, T. S. (2004). A classification of landscape fire succession models: Spatial simulations of fire and vegetation dynamics. *Ecological Modelling*, *179*(1), 3–27. doi: 10.1016/j.ecolmodel.2004.03.015

Keeley, J. E., & Syphard, A. D. (2019). Twenty-first century California, USA, wildfires: Fuel-dominated vs. wind-dominated fires. *Fire Ecology*, *15*(1). doi: 10.1186/s42408-019-0041-0

Kolden, C. A., Abatzoglou, J. T., Jones, M. W., & Jain, P. (2024). Wildfires in 2023. *Nature Reviews Earth & Environment*, *5*(4), 238–240. doi: 10.1038/s43017-024-00544-y

Lasslop, G., Hantson, S., & Kloster, S. (2015). Influence of wind speed on the global variability of burned fraction: A global fire model's perspective. *International Journal of Wildland Fire*, *24*(7), 989. doi: 10.1071/wf15052

Lautenberger, C. (2013). Wildland fire modeling with an Eulerian level set method and automated calibration. Fire Safety Journal, 62, 289-298. doi: 10.1016/j.firesaf.2013.08.014

La Puma, I.P. (2023). LANDFIRE technical documentation: U.S. Geological Survey Open-File Report 2023–1045, 103. doi: 10.3133/ofr20231045

Loehman, R. A., Keane, R. E., & Holsinger, L. M. (2020). Simulation modeling of complex climate, Wildfire, and vegetation dynamics to address wicked problems in Land Management. *Frontiers in Forests and Global Change*, *3*. doi: 10.3389/ffgc.2020.00003

Moritz, M. A., Morais, M. E., Summerell, L. A., Carlson, J. M., & Doyle, J. (2005). Wildfires, complexity, and highly optimized tolerance. *Proceedings of the National Academy of Sciences*, *102*(50), 17912–17917. doi: 10.1073/pnas.0508985102

Osher, S., & Sethian, J. A. (1988). Fronts propagating with curvature-dependent speed: Algorithms based on Hamilton-Jacobi formulations. *Journal of Computational Physics*, *79*(1), 12–49. doi: 10.1016/0021-9991(88)90002-2

Pfeiffer, M., Spessa, A., & Kaplan, J. O. (2013). A model for global biomass burning in preindustrial time: LPJ-LMfire (v1.0). *Geoscientific Model Development*, *6*(3), 643–685. doi: 10.5194/gmd-6-643-2013

Pyne, S J, Andrews, P. L., & Laven, R. D. (1996). Fire Behavior. In *Introduction to wildland fire* (2nd ed., pp. 49). Wiley.

Rabin, S. S., Melton, J. R., Lasslop, G., Bachelet, D., Forrest, M., Hantson, S., Kaplan, J. O., Li, F., Mangeon, S., Ward, D. S., Yue, C., Arora, V. K., Hickler, T., Kloster, S., Knorr, W., Nieradzik, L., Spessa, A., Folberth, G. A., Sheehan, T., … Arneth, A. (2017). The fire modeling intercomparison project (firemip), phase 1: Experimental and analytical protocols with detailed model descriptions. *Geoscientific Model Development*, *10*(3), 1175–1197. doi: 10.5194/gmd-10-1175-2017

Rehm, R. G., & Mell, W. E. (2009). A simple model for wind effects of burning structures and topography on wildland–urban interface surface-fire propagation. International Journal of Wildland Fire, 18(3), 290–301. doi: 10.1071/WF08087

Ritter, S. M., Hoffman, C. M., Battaglia, M. A., Linn, R., & Mell, W. E. (2023). Vertical and horizontal crown fuel continuity influences group-scale ignition and fuel consumption. *Fire*, *6*(8), 321. doi: 10.3390/fire6080321

Scott, J. H., & Burgan, R. E. (2005). Standard fire behavior fuel models: A comprehensive set for use with Rothermel's surface fire spread model. *Fort Collins, CO: USDA Forest Service, Rocky Mountain Research Station.*, *RMRS-GTR-153*. doi: 10.2737/rmrs-gtr-153

van Wees, D., van der Werf, G. R., Randerson, J. T., Rogers, B. M., Chen, Y., Veraverbeke, S., Giglio, L., & Morton, D. C. (2022). Global biomass burning fuel consumption and emissions at 500 m spatial resolution based on the global fire emissions database (GFED). *Geoscientific Model Development*, *15*(22), 8411–8437. doi: 10.5194/gmd-15-8411-2022

Appendix A.

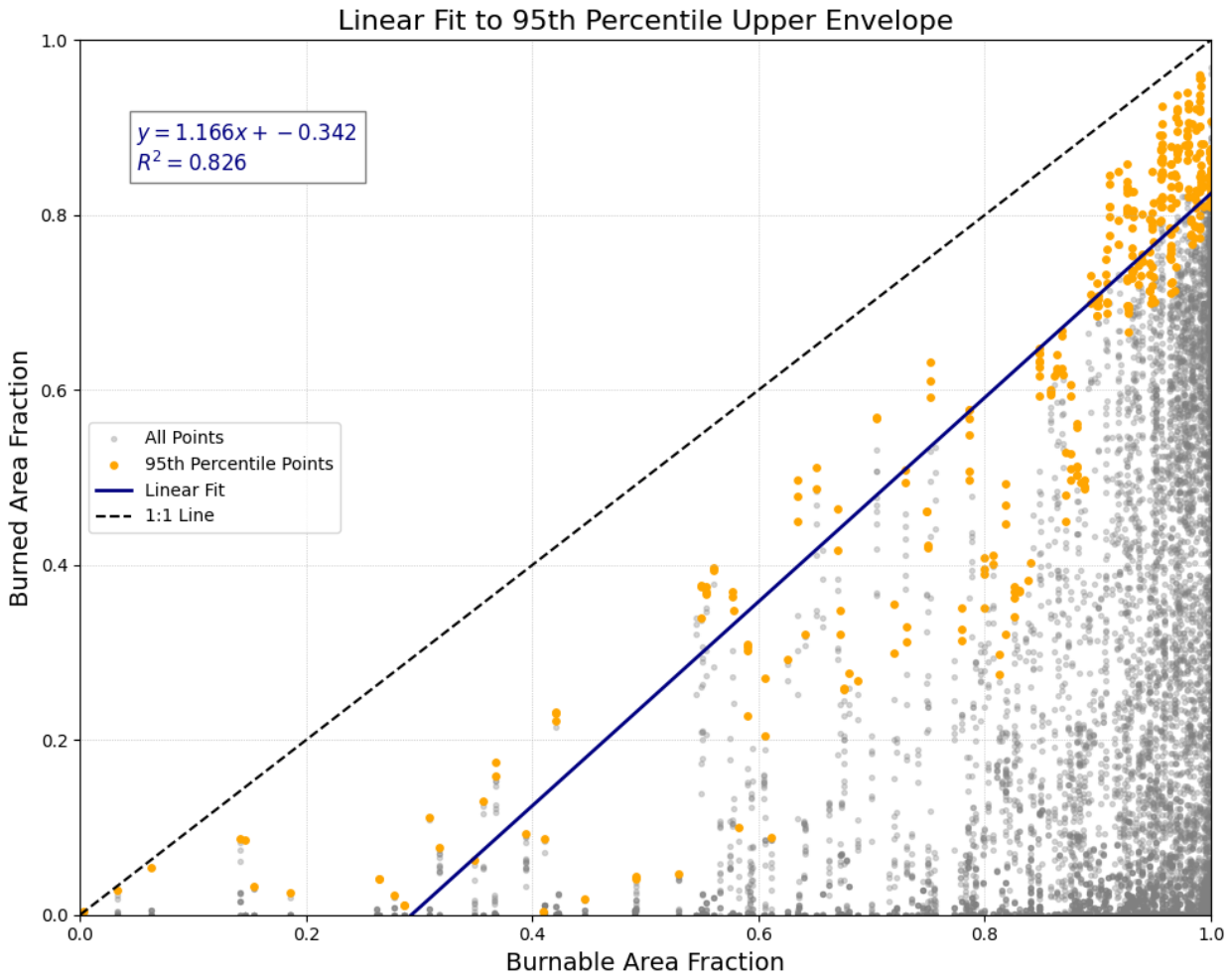

Figure A.1. Linear fit to the 95th percentile upper envelope of burned area fraction, binned by burnable area fraction.

Orange points represent tile-level burned area values in the top 5% within each 1% burnable area bin (n = 7,984). The fitted line ($R^2 = 0.826$) represents the potential upper limit of fire spread, given high fuel availability and favorable alignment. This envelope provides a reference for assessing fire spread limitations due to fragmentation, terrain, or other constraints.

Mann–Whitney U-Test (Two-Sided)
Adjusted Burned Area by Wind Speed

Low Fragmentation

	15	30	45	60
15		0.000*	0.000*	0.000*
30	0.000*		0.000*	0.000*
45	0.000*	0.000*		0.074
60	0.000*	0.000*	0.074	

High Fragmentation

	15	30	45	60
15		0.336	0.084	0.073
30	0.336		0.429	0.391
45	0.084	0.429		0.921
60	0.073	0.391	0.921	

Figure A.2. Pairwise two-sided Mann–Whitney U-test results comparing adjusted burned area fractions across wind speeds, stratified by fragmentation level.

Each cell displays the p-value for the comparison between wind speeds. Asterisks (*) indicate statistical significance at $p < 0.05$. In low-fragmentation (high continuity) landscapes, most wind speed comparisons show significant differences in fire spread, while high-fragmentation areas show no significant change in burned area with increasing wind.

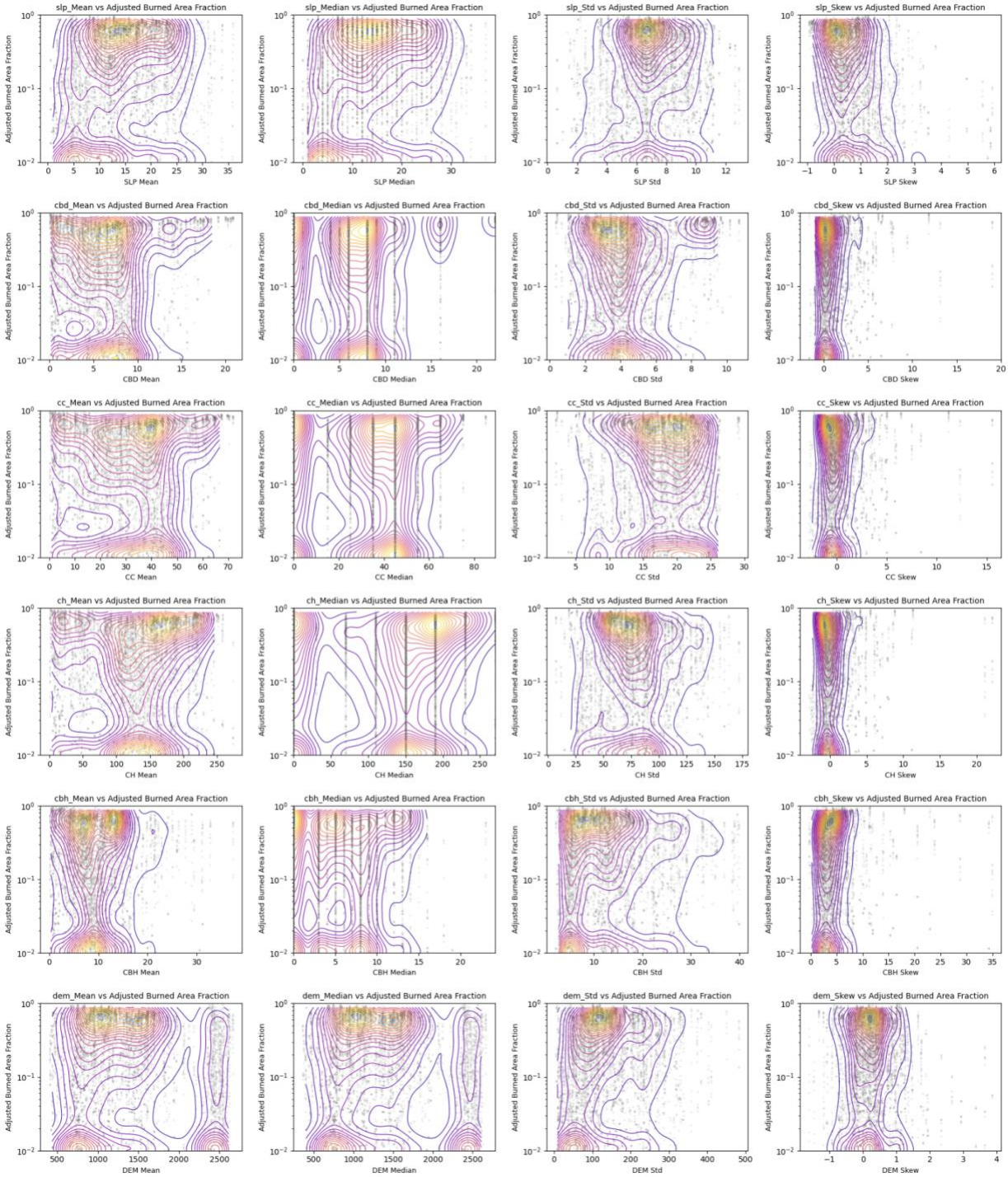

Figure A.3. Joint distributions of structural/environmental metrics and adjusted burned area fraction across all tiles.

Contours represent 2D kernel density estimates between each variable-statistic combination (x-axis) and adjusted burned area fraction (y-axis, log-scaled). While no strong bivariate relationships emerge, these

variables informed spatial heterogeneity in fire spread potential and were used in data filtering and characterization throughout the study.